Highly sensitive detection of influenza virus by boron-doped diamond electrode terminated with sialic acid-mimic peptide

Teruhiko Matsubara[a], Michiko Ujie[a], Takashi Yamamoto[b], Miku Akahori[b], Yasuaki Einaga[b,c], and Toshinori Sato[a,1]

[a]Department of Biosciences and Informatics, Faculty of Science and Technology, Keio University, Kohoku-ku, Yokohama, Kanagawa 223-8522, Japan; [b]Department of Chemistry, Faculty of Science and Technology, Keio University, Kohoku-ku, Yokohama, Kanagawa 223-8522, Japan; and [c]JST-ACCEL, Kohoku-ku, Yokohama, Kanagawa 223-8522, Japan

Edited by Thomas E. Mallouk, The Pennsylvania State University, University Park, PA, and approved June 17, 2016 (received for review March 3, 2016)

The progression of influenza varies according to age and the presence of an underlying disease; appropriate treatment is therefore required to prevent severe disease. Anti-influenza therapy, such as with neuraminidase inhibitors, is effective, but diagnosis at an early phase of infection before viral propagation is critical. Here, we show that several dozen plaque-forming units (pfu) of influenza virus (IFV) can be detected using a boron-doped diamond (BDD) electrode terminated with a sialic acid-mimic peptide. The peptide was used instead of the sialyloligosaccharide receptor, which is the common receptor of influenza A and B viruses required during the early phase of infection, to capture IFV particles. The peptide, which was previously identified by phage-display technology, was immobilized by click chemistry on the BDD electrode, which has excellent electrochemical characteristics such as low background current and weak adsorption of biomolecules. Electrochemical impedance spectroscopy revealed that H1N1 and H3N2 IFVs were detectable in the range of 20–500 pfu by using the peptide-terminated BDD electrode. Our results demonstrate that the BDD device integrated with the receptor-mimic peptide has high sensitivity for detection of a low number of virus particles in the early phase of infection.

influenza virus | boron-doped diamond electrode | sialic acid-mimic peptide | electrochemical impedance spectroscopy | click chemistry

Seasonal H1N1 and H3N2 virus subtypes circulate every year, resulting in widespread influenza (1, 2). High-risk patients (e.g., young children, the elderly, and individuals with underlying disease) are more likely to develop severe influenza. A clinical diagnosis can be made with a rapid immunochromatography test kit consisting of a monoclonal antibody against influenza virus (IFV) (3, 4) that is used to analyze swab samples collected from patients; however, it is not sufficiently sensitive to diagnose early stages of influenza. Early detection is critical, as neuraminidase (NA) inhibitor therapy is effective within 30 h of the onset of symptoms (5, 6).

Type A virus is classified into subtypes on the basis of the antigenicity of hemagglutinin (HA) and NA; to date, 16 HA and nine NA subtypes have been identified (7). Sialylgalactose (Neu5Ac-Gal) is the common receptor of influenza HA in all subtypes in the same animal; as such, sialyloligosaccharides have been used to detect HAs and IFVs (8, 9). Electrodes immobilized with α2-3- or α2-6-sialylated groups can distinguish between H1N1 and H5N1 HA (10) or H1N1 and H5N9 virus (11). A boron-doped diamond (BDD) electrode was recently developed and has shown excellent electrochemical characteristics, including a broad range of electrochemical potentials, low background current, and weak adsorption of biomolecules compared with conventional electrode materials such as glassy carbon (GC) or platinum (12). BDD electrodes can detect biomolecules such as glutathione (13) and reduced nicotinamide adenine dinucleotide (14) and have been applied to the diagnosis of stomach disorders on the basis of detection of pH changes (13). In the present study, a sialic acid-mimic peptide was immobilized on a BDD electrode by click chemistry for electrochemical detection of IFV (Fig. 1). The sialic acid-mimic pentapeptide Ala-Arg-Leu-Pro-Arg was identified by serial selection from random peptide libraries, using phage-display technology (15). In contrast to the standard sialyloligosaccharide receptor, this peptide was predicted to be able to capture HA and, hence, IFV (16, 17): When IFV is incubated with a sialylated electrode, NA digestion of the electrode-bound sialyloligosaccharide can reduce the sensitivity of IFV detection, whereas the sialic acid-mimic peptide is free from risk for NA digestion.

Results and Discussion

Alkyne-Terminated BDD Electrode. A thin BDD film was prepared by microwave plasma-assisted vapor deposition on a Si(111) wafer substrate; its polycrystalline structure was confirmed by field emission scanning electron microscopy (Fig. 2*A*). The form of the diamond was verified by Raman spectroscopic analysis, using a 532-nm wavelength light (18), and a sharp sp^3 peak corresponding to diamond was observed at 1,332 cm^{-1} (Fig. S1*A*). The triisopropylsilyl-protected ethynyl aryl group (TIPS-Eth-Ar) was immobilized onto the BDD surface by electroreduction (Fig. S1*B*) (19). The reduction peak at −0.01 V was clearly observed in the first cycle of the cyclic voltammogram (Fig. S1*C*), and blocking of the electric charge transfer between BDD and a bulky TIPS-Eth-Ar was observed in the second or a later cycle. To expose the Eth group, the TIPS group was deprotected, and recovery of the blocking properties was confirmed by cyclic voltammetry (alkyne-terminated BDD; Fig. S1*D*).

Significance

A large number of people suffer from influenza every year. Early detection is critical for preventing severe influenza in high-risk groups. There is usually not enough time to produce vaccines against pandemic viruses before they spread to other countries. Anti-influenza therapy using neuraminidase inhibitors is effective within 30 h of the onset of symptoms. Here we show that several dozen plaque-forming units of influenza virus (IFV) are detectable by a boron-doped diamond electrode terminated with a sialic acid-mimic peptide with the ability to capture IFV. The electrode was sufficiently sensitive to detect IFV in specimens obtained in the early phase of infection. The device developed in the present work has potential applications in the highly sensitive detection of IFV to fight against influenza.

Author contributions: T.M. and T.S. designed research; T.M. and M.U. performed research; T.Y., M.A., and Y.E. contributed new reagents/analytic tools; T.M., M.U., T.Y., and Y.E. analyzed data; and T.M. and T.S. wrote the paper.

The authors declare no conflict of interest.

This article is a PNAS Direct Submission.

[1]To whom correspondence should be addressed. Email: sato@bio.keio.ac.jp.

This article contains supporting information online at www.pnas.org/lookup/suppl/doi:10.1073/pnas.1603609113/-/DCSupplemental.

BIOCHEMISTRY

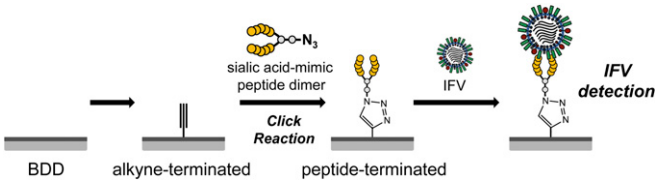

Fig. 1. Schematic illustration of the preparation of a peptide-terminated BDD electrode and IFV detection. The sialic acid-mimic peptide dimer was immobilized on the alkyne-terminated BDD electrode via a click reaction. IFV capture was detected electrochemically.

Click Reaction of Peptide with Alkyne-Terminated BDD Electrode. To improve the affinity of the peptide for the HA of IFV, a dimer of the sialic acid-mimic peptide with a branched lysine (Lys) core [(Ala-Arg-Leu-Pro-Arg)$_2$Lys-Lys(N$_3$)] was chemically synthesized (*SI Methods* and Fig. S2*A*) (20, 21). This peptide dimer had an azide Lys with an azido side chain (N$_3$) at the carboxyl terminal of the Lys core. For the click reaction, the alkyne-terminated BDD electrode was incubated with the azide-conjugated peptide for 24 h. After washing, the electrode was dried (peptide-terminated BDD; Fig. 2*B*). Fig. 2*C* shows the cyclic voltammograms of 10 mM $[Fe(CN)_6]^{3-/4-}$, using BDD electrodes before and after modification. The bare BDD electrode had a quasi-reversible voltammogram, with two peaks representing the oxidation and reduction of $[Fe(CN)_6]^{3-/4-}$. For the Eth-Ar-modified BDD electrode, the separation between the oxidation and reduction peaks was larger, and the height of the peaks was reduced. Because $[Fe(CN)_6]^{3-/4-}$ molecules in solution can easily reach the electrode surface, the changes in the peaks indicated that the Eth-Ar layer acted as a barrier for electric charge transfer. The height of the peaks of the peptide-terminated BDD electrode was even lower. The peptide immobilization was further confirmed by water contact angle hysteresis and X-ray photoelectron spectroscopy. The values of the contact angle decreased from 68° for the bare BDD to 50° and 47° for the Eth-Ar- and peptide-terminated BDD, respectively (Fig. 2*D*). These results indicated that the bare BDD surface was converted to a hydrophilic surface on which the peptide was immobilized. In addition, the X-ray photoelectron spectroscopy spectrum of the peptide-terminated BDD showed a strong N(1s) peak derived from the peptide and triazole ring (Fig. S1*E*), indicating formation of the peptide-terminated BDD (19).

Estimation of Amount of Peptide on BDD Electrode. To estimate the surface coverage of peptide immobilized on the BDD electrode, a ferrocene-containing peptide dimer was immobilized (Fig. 2*E*) (22). Two ferrocenyl groups were attached to the N terminus of the peptide dimer (Fig. S2*B*) (23). The ferrocenyl peptide-terminated BDD electrode showed a well-defined ferrocene/ferrocenium redox system (Fig. 2*F*). The anodic and cathodic peak current densities (i_{pa} and i_{pc}) were proportional to the potential sweep rate (Fig. 2*G*), and the i_{pa}/i_{pc} ratio was close to unity. These characteristics indicated that the redox process on the electrodes was controlled by charge-transfer kinetics, confirming that the ferrocenyl peptide was immobilized on the BDD surface (24).

The oxidation current was integrated to estimate surface coverage (Fig. 2*F*). The amount of ferrocenyl peptide immobilized on BDD electrode was around 0.11 pmol/cm^2 (Q = 0.021 μC/cm^2), according to the gray area of the oxidation peak between 0.28 and 0.50 V. This value was about four times lower than that of a grafted ferrocene on a GC electrode (0.44 pmol/cm^2) (22). On the basis of the surface coverage of peptide immobilized on the BDD electrode, the density of peptide was calculated as 5.4 molecules per 100 nm^2 (i.e., 10,000 nm^2, with a distance between peptides of about 42 nm). Because the size of IFV is 80–120 nm, peptide

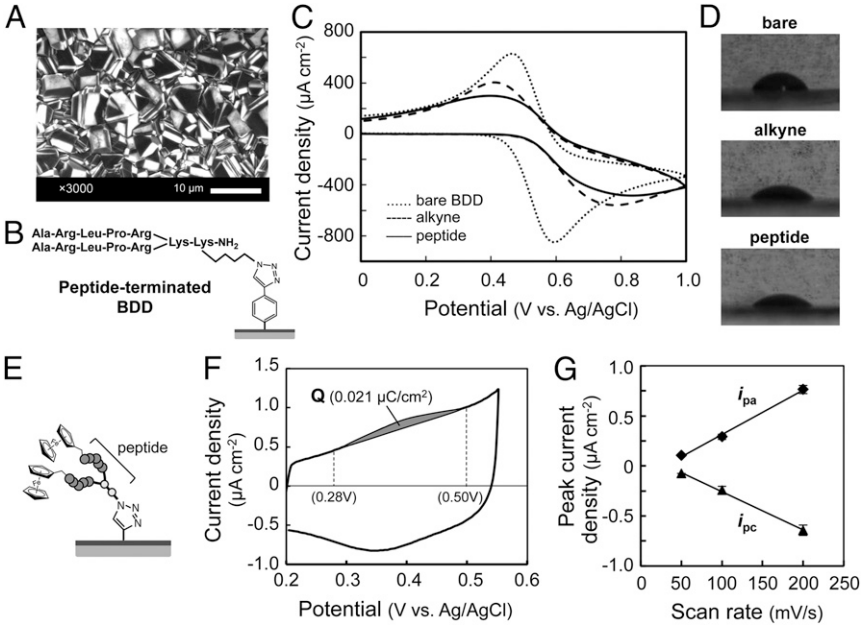

Fig. 2. Preparation of BDD electrodes modified with sialic acid-mimic peptide. (*A*) Scanning electron micrograph of the BDD electrode. (*B*) Structure of peptide-terminated BDD. The azide-containing peptide (Ala-Arg-Leu-Pro-Arg)$_2$Lys-Lys(N$_3$) was immobilized on an alkyne-terminated BDD electrode via a click reaction. (*C*) Cyclic voltammograms of 10 mM K$_3$[Fe(CN)$_6$] using bare (dotted line), alkyne-terminated (dashed line), and peptide-terminated (solid line) BDD electrodes in 100 mM Na$_2$SO$_4$. The sweep rate was 100 mV/s. (*D*) Water contact angle images for bare (68°; *Upper*), alkyne-terminated (50°; *Center*), and peptide-terminated (47°; *Lower*) BDD electrodes. (*E*) Structure of a ferrocenyl peptide-terminated BDD electrode. (*F*) Cyclic voltammogram of a ferrocenyl peptide-terminated BDD electrode in PBS. The amount of ferrocenyl peptide immobilized on the electrode (0.11 pmol/cm^2) was estimated from the gray area of the oxidation peak (0.021 μC/cm^2) between 0.28 and 0.50 V. The sweep rate was 200 mV/s. (*G*) Potential sweep rate dependence of anodic and cathodic peak current densities (i_{pa} and i_{pc}).

coverage was considered to be sufficient to form an IFV monolayer on the BDD surface.

Selective Detection of HA on Peptide-Terminated BDD by EIS. For HA detection, the peptide-terminated BDD surface was incubated with HA in PBS for 15 min. The BDD electrode was washed with PBS, and electrochemical impedance spectroscopy (EIS) was carried out, using 5 mM $[Fe(CN)_6]^{3-/4-}$ in PBS as a redox probe. Fig. 3*A* shows the spectra obtained for 5–375 nM HA, using the peptide-terminated BDD electrode. With increasing HA concentration, the diameter of the Nyquist plots increased, where the diameter of the semicircle represents charge transfer resistance (R_{ct}) on the electrode surface. The HA-bound layer decreased charge transfer for the redox probe. A plot of protein concentration versus R_{ct} values revealed a slope that was significantly larger for HA than for BSA (Fig. 3*B*). These results indicated that the peptide-terminated BDD electrode selectively detected HA.

A peptide-terminated GC electrode was also prepared, and the binding of HA was evaluated by EIS (22). The amount of ferrocenyl peptide immobilized on the GC electrode was 1.3 pmol/cm^2 (Q = 0.25 μC/cm^2; Fig. S3 *A* and *B*), which was 12 times greater than that on the peptide-terminated BDD electrode (0.11 pmol/cm^2; Fig. 2*F*). Despite the large amount of peptides on the modified GC electrode, the R_{ct} values did not increase as a function of HA concentration (Fig. S3*C*), indicating that the BDD electrode was superior for HA detection. BSA is known to adsorb onto the surface of GC, but not onto that of the BDD electrodes (25). This protein adsorption suppresses electrochemical responses (26). We therefore considered that HA and BSA adsorb equally onto the GC surface, regardless of the efficiency of peptide immobilization, resulting in no selective binding of HA to the peptide-terminated GC electrode.

Highly Sensitive Detection of IFV by EIS. Seasonal H1 and H3 subtypes of influenza A virus were analyzed by EIS, using the peptide-terminated BDD electrode. The viral titer of IFV stock was determined by the plaque assay, using Mardin-Darby canine kidney epithelial cells (15). The IFV stock solution was thawed and diluted with PBS, and the electrode was incubated in H1N1 solution (1–400 pfu) for 45 min. After washing the electrode with PBS, EIS was carried out using 5 mM $[Fe(CN)_6]^{3-/4-}$ in PBS. The diameter of the Nyquist plots increased in the 20–400 pfu range, but there was no increase in R_{ct} values for the Lys-terminated BDD electrode (Fig. 3 *C* and *D*) prepared by modifying BDD with Lys(N_3) without peptide, thereby confirming the peptide-mediated detection of IFV. Fig. 3*E* shows the difference in ΔR_{ct} values between peptide- and Lys-terminated BDD electrodes; ΔR_{ct} values were higher for the H1N1 than for the H3N2 subtype (400 pfu; 9,230 and 2,215 ohm, respectively), demonstrating that the peptide-terminated BDD electrode could quantitatively detect both H1N1 and H3N2 IFVs at 20–400 pfu.

Conclusion and Future Perspective. Using the combination of sialic acid-mimic peptide and BDD electrode, the range of IFV detection observed here (400–8,000 pfu/mL, or 20–400 pfu in 50 μL) indicated that the peptide-terminated BDD electrode could detect IFV in nasal wash specimens (400–10,000 pfu/mL) with high sensitivity (27). EIS studies of inactivated IFVs (H1N1 and H3N2) have recently been carried out using sialyl galactoside-immobilized (11) and antibody-immobilized (28) electrodes; although IFVs were detected, viral titers were reported in micrograms per milliliter, making it difficult to compare the limits of IFV detection with our findings. The specimens obtained from patients were broadly evaluated, using an immunochromatography test kit for the rapid diagnosis of influenza. The kit did not require any additional equipment (4). However, to improve the detection, an expensive apparatus, such as a fluorescence detector, is required (3). We are constantly exposed to not only seasonal but also highly pathogenic viruses such as H5N1 and H7N9 (1). The peptide-terminated BDD electrode developed here has potential applications in the early diagnosis of influenza and in anti-influenza therapy in the event of a pandemic.

Methods

Materials. HAs used in the study were provided by Yujiro Suzuki (Kitasato Institute). HA H1 and H3 subtypes were prepared from influenza A/New Caledonia/20/99 (H1N1) and A/New York/55/2004 (H3N2) viruses, respectively (29). The A/Puerto Rico/8/34 (H1N1) and A/Aichi/2/68 (H3N2) IFVs have been previously described (15). IFVs were grown in allantoic sacs of 11-d-old embryonated eggs and resuspended in 10 mM Tris·HCl (pH 7.8) containing 1 mM DTT and 20% (wt/vol) glycerol and stored at −80 °C until use (30).

BDD Electrode. A thin BDD film was deposited onto a Si(111) wafer substrate (5-cm diameter) in a microwave plasma-assisted vapor deposition system

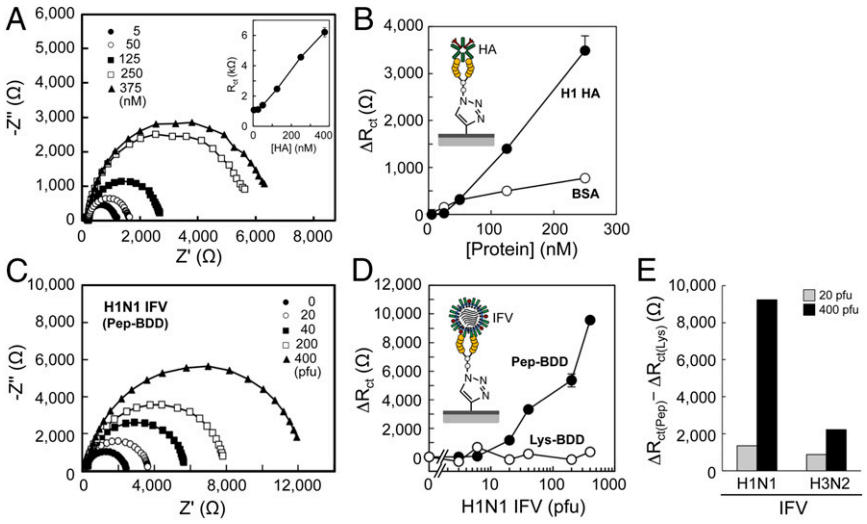

Fig. 3. Detection of H1 HA and IFV on the peptide-terminated BDD electrode by EIS. (*A*) Representative Nyquist plots of HA on the peptide-terminated BDD electrode. The R_{ct} value is plotted as a function of HA concentration (*Inset*). (*B*) Change in R_{ct} (ΔR_{ct}) as a function of HA concentration in PBS. (*C*) Representative Nyquist plots of H1N1 (A/Puerto Rico/8/34) IFV on the peptide-terminated BDD electrode. (*D*) Dependence of ΔR_{ct} on the number of IFVs in PBS. (*E*) Peptide-mediated detection of IFVs on the peptide-terminated BDD electrode. Pep-BDD, peptide-terminated BDD; Lys-BDD, Lys-terminated BDD.

(AX6500; CORNES Technologies Corp.). Acetone and trimethoxyborane gas were used as carbon and boron sources, respectively, at an atomic ratio of B/C = 0.3%. Deposition was carried out for 8 h under 85 Torr chamber pressure, 5,000 W microwave power, and 900–1,000 °C substrate temperature. Surface morphology was characterized by field-emission scanning electron microscopy (JSM-7600; JEOL). Raman spectra were obtained in ambient air at room temperature under excitation at 532 nm from a green laser diode (ST-BX51; Seki Technotron Corp.). The wafer was divided into two pieces for further electrochemical experiments (bare BDD).

Electrochemical Measurements. Cyclic voltammetry (CV) and EIS were carried out with a standard three-electrode configuration, using a potentiostat (CompactStat; Ivium Technologies). The BDD electrode used as the working electrode was assembled as the bottom (2-cm diameter) of a single-compartment cell. An Ag/AgCl (saturated KCl) electrode and Pt wire electrode were used as the reference (+0.199 V vs. standard hydrogen) and counter electrodes, respectively. EIS measurements were carried out at the equilibrium or open circuit potential without bias voltage in the frequency range of 5 Hz–50 kHz and a 25-mV amplitude.

Deposition of Alkynyl Group onto the BDD Surface. To obtain alkyne-terminated BDD, the surface (diameter of 2.08 cm) was modified (Fig. S1*B*) (19) by electroreduction via CV with a scan rate of 50 mV/s for five cycles between +0.60 V and −0.70 V in acetonitrile solution containing 100 mM TIPS-protected Eth-Ar diazonium salt and 100 mM tetrabutylammonium hexafluorophosphate (Bu_4NPF_6). An electroreduction peak was observed at −0.01 V (Fig. S1*C*); the peak current disappeared after the second cycle, indicating that electron transfer between BDD and the bulky TIPS-protected Eth-Ar group was blocked. The TIPS group was deprotected by immersing the TIPS-terminated BDD in a tetrahydrofuran solution of tetra-*n*-butylammonium fluoride (50 mM) for 20 min at room temperature, yielding alkyne-terminated BDD.

The electrochemical behavior of BDD electrodes was monitored by CV in an acetonitrile solution of 1 mM ferrocene and 0.1 M Bu_4NPF_6, with a scan rate of 100 $mV{\cdot}s^{-1}$ between +1.0 and −0.50 V (vs. Ag/AgCl). CVs of a ferrocene redox reaction were almost identical for bare (dotted line) and alkyne-terminated (solid line) BDD electrodes (Fig. S1*D*). In contrast, decreases in both oxidation and reduction peak currents were observed for TIPS-terminated BDD electrodes, and the separation of peak-to-peak potentials was larger than for bare BDD (Fig. S1*D*; broken line). These results indicated that bulky TIPS groups blocked electron transfer between BDD and ferrocene in solution.

Click Chemistry and Electrode Properties. The peptide dimer was immobilized on the alkyne-terminated BDD by click chemistry. The alkyne-terminated BDD (1/8 cut) electrode was incubated for 24 h in a solution of 0.1 mM peptide, 0.8 mM $CuSO_4$, 0.5 mM sodium ascorbate, and 0.1 mM Tris(benzyltriazolylmethyl) amine in 1 mL methanol:water (0.375:0.625). The electrode was washed with water, ethanol, and acetone and dried under N_2 gas, yielding peptide-terminated BDD. The electrochemical measurements were performed within a few days after the preparation of the peptide-terminated BDD.

The blocking properties of each layer on the BDD electrode were characterized by recording the CV of ferrocene oxidation after each modification step. CVs of bare and alkyne- and peptide-terminated BDD electrodes were recorded in 100 mM Na_2SO_4 containing 10 mM $K_3[Fe(CN)_6]$ with a scan rate of 100 $mV{\cdot}s^{-1}$ between 0 V and +1.0 V (vs. Ag/AgCl) (Fig. 2*C*). CVs of ferrocenyl peptide-terminated BDD electrodes were recorded in Dulbecco's PBS (pH 7.4) with a scan rate of 200 $mV{\cdot}s^{-1}$ between +0.2 V and +0.55 V (vs. Ag/AgCl) (Fig. 2 *E* and *F*). Water contact angle measurements were carried out to assess the hydrophilic/hydrophobic nature of the electrode before and after peptide modification by the sessile drop method.

Surface Coverage of Peptide on BDD Surface. Surface coverage by the peptide was estimated by click reaction with a ferrocenylpeptide dimer instead of the peptide dimer (Fig. 2*E*). Two ferrocenyl groups were linked to the N terminus of the peptide dimer (Fig. S2*B*). The total coverage of the BDD surface by the peptide (Γ_{pep}) was determined from the integration of the area under the oxidation peak at low scan rates yielding the charge passed (Q) (Fig. 2*F*), according to the equation $\Gamma_{pep} = Q/(nFA)$ (22), where n is the number of electrons involved in the reaction, F is the Faraday constant, and A is the electro-active surface area of the peptide-terminated BDD electrode. The typical Γ_{pep} value was estimated to be 0.11 $pmol/cm^2$.

HA and IFV Detection by EIS. The peptide-terminated BDD electrode (2-mm diameter) was incubated for 50 μL of a solution consisting of HA, BSA, or IFV in PBS (pH 7.4) for 15 min (HA and BSA) or 45 min (IFV). The electrode was washed with PBS, and EIS measurements were carried out using PBS containing a mixture of 5 mM $Fe(CN)^{4-}$ (ferrocyanide) and 5 mM $Fe(CN)^{3-}$ (ferricyanide) as redox probes.

ACKNOWLEDGMENTS. This study was supported by Japan Society for the Promotion of Science Kakenhi Grants 22790115 and 15K01806 (to T.M.) and Grants 23106726 and 26560245 (to T.S.).

1. Webster RG, Govorkova EA (2014) Continuing challenges in influenza. *Ann N Y Acad Sci* 1323:115–139.
2. Salomon R, Webster RG (2009) The influenza virus enigma. *Cell* 136(3):402–410.
3. Sakurai A, Shibasaki F (2012) Updated values for molecular diagnosis for highly pathogenic avian influenza virus. *Viruses* 4(8):1235–1257.
4. Sasaki T, et al. (2012) Reliability of a newly-developed immunochromatography diagnostic kit for pandemic influenza A/H1N1pdm virus: Implications for drug administration. *PLoS One* 7(11):e50670.
5. Hayden FG, et al. (1997) Efficacy and safety of the neuraminidase inhibitor zanamivir in the treatment of influenzavirus infections. GG167 Influenza Study Group. *N Engl J Med* 337(13):874–880.
6. von Itzstein M (2007) The war against influenza: Discovery and development of sialidase inhibitors. *Nat Rev Drug Discov* 6(12):967–974.
7. Gamblin SJ, Skehel JJ (2010) Influenza hemagglutinin and neuraminidase membrane glycoproteins. *J Biol Chem* 285(37):28403–28409.
8. Matrosovich M, Klenk HD (2003) Natural and synthetic sialic acid-containing inhibitors of influenza virus receptor binding. *Rev Med Virol* 13(2):85–97.
9. Hatano K, Matsuoka K, Terunuma D (2013) Carbosilane glycodendrimers. *Chem Soc Rev* 42(11):4574–4598.
10. Hideshima S, et al. (2013) Attomolar detection of influenza A virus hemagglutinin human H1 and avian H5 using glycan-blotted field effect transistor biosensor. *Anal Chem* 85(12):5641–5644.
11. Wicklein B, et al. (2013) Biomimetic architectures for the impedimetric discrimination of influenza virus phenotypes. *Adv Funct Mater* 23(2):254–262.
12. Luong JH, Male KB, Glennon JD (2009) Boron-doped diamond electrode: Synthesis, characterization, functionalization and analytical applications. *Analyst (Lond)* 134(10):1965–1979.
13. Fierro S, et al. (2012) In vivo assessment of cancerous tumors using boron doped diamond microelectrode. *Sci Rep* 2:901.
14. Oyobiki R, et al. (2014) Toward high-throughput screening of NAD(P)-dependent oxidoreductases using boron-doped diamond microelectrodes and microfluidic devices. *Anal Chem* 86(19):9570–9575.
15. Matsubara T, et al. (2010) Sialic acid-mimic peptides as hemagglutinin inhibitors for anti-influenza therapy. *J Med Chem* 53(11):4441–4449.
16. Matsubara T (2012) Potential of peptides as inhibitors and mimotopes: Selection of carbohydrate-mimetic peptides from phage display libraries. *J Nucleic Acids* 2012:740982.
17. Hatano K, et al. (2014) Synthesis and influenza virus inhibitory activities of carbosilane dendrimers peripherally functionalized with hemagglutinin-binding Peptide. *J Med Chem* 57(20):8332–8339.
18. Ruther RE, et al. (2011) Highly stable redox-active molecular layers by covalent grafting to conductive diamond. *J Am Chem Soc* 133(15):5692–5694.
19. Natsui K, Yamamoto T, Akahori M, Einaga Y (2015) Photochromism-induced amplification of critical current density in superconducting boron-doped diamond with an azobenzene molecular layer. *ACS Appl Mater Interfaces* 7(1):887–894.
20. Crespo L, et al. (2005) Peptide and amide bond-containing dendrimers. *Chem Rev* 105(5):1663–1681.
21. Tam JP (1988) Synthetic peptide vaccine design: Synthesis and properties of a high-density multiple antigenic peptide system. *Proc Natl Acad Sci USA* 85(15):5409–5413.
22. Leroux YR, Fei H, Noël JM, Roux C, Hapiot P (2010) Efficient covalent modification of a carbon surface: Use of a silyl protecting group to form an active monolayer. *J Am Chem Soc* 132(40):14039–14041.
23. Kira M, Matsubara T, Shinohara H, Sisido M (1997) Synthesis and redox property of polypeptides containing L-ferrocenylalanine. *Chem Lett* 26(1):89–90.
24. Kondo T, et al. (2014) Direct determination of chemical oxygen demand by anodic decomposition of organic compounds at a diamond electrode. *Anal Chem* 86(16):8066–8072.
25. Shin D, Tryk DA, Fujishima A, Merkoçi A, Wang J (2005) Resistance to surfactant and protein fouling effects at conducting diamond electrodes. *Electroanalysis* 17(4):305–311.
26. Downard AJ, Roddick AD (1995) Protein adsorption at glassy carbon electrodes: The effect of covalently bound surface groups. *Electroanalysis* 7(4):376–378.
27. Suess T, et al. (2012) Comparison of shedding characteristics of seasonal influenza virus (sub)types and influenza A(H1N1)pdm09; Germany, 2007-2011. *PLoS One* 7(12):e51653.
28. Hassen WM, Duplan V, Frost E, Dubowski JJ (2011) Quantitation of influenza A virus in the presence of extraneous protein using electrochemical impedance spectroscopy. *Electrochim Acta* 56(24):8325–8328.
29. Asahi Y, et al. (2002) Protection against influenza virus infection in polymeric Ig receptor knockout mice immunized intranasally with adjuvant-combined vaccines. *J Immunol* 168(6):2930–2938.
30. Yamanaka K, Ishihama A, Nagata K (1990) Reconstitution of influenza virus RNA-nucleoprotein complexes structurally resembling native viral ribonucleoprotein cores. *J Biol Chem* 265(19):11151–11155.
31. Matsubara T, et al. (2009) Inhibition of influenza virus infections by sialylgalactose-binding peptides selected from a phage library. *J Med Chem* 52(14):4247–4256.
32. Schneggenburger PE, Worbs B, Diederichsen U (2010) Azide reduction during peptide cleavage from solid support-the choice of thioscavenger? *J Pept Sci* 16(1):10–14.